

# Data Analysis for the GN2 B-Tagging Algorithm using Pythia8 and Herwig7 samples on $t\bar{t}$ and $Z'$ events

Salvador Torpes<sup>1,a</sup>

Project Supervisor: Helena Santos (LIP)

<sup>1</sup>Instituto Superior Técnico, Lisboa, Portugal

## Abstract.

Our research focuses on evaluating the performance of the GN2 (2nd generation Graphical Neural Learning) B-tagging Algorithm. To accomplish this, we conducted experiments using two Monte Carlo (MC) Generators: Pythia8 and Herwig. Both generators were tested with  $t\bar{t}$  and  $Z'$  samples. The main objective of our study is to compare the outcomes of the newly implemented Herwig generator with those obtained from Pythia, enabling us to verify whether the effectiveness and efficiency of this novel algorithm is sensitive to different parton shower phenomenological models. Our analysis centers around histograms that showcase a comparative evaluation of various jets and tracks variables derived from the Pythia and Herwig samples. These histograms provide valuable insights into the performance differences between the two generators and offer a comprehensive understanding of their strengths and weaknesses. Some of the variables analysed are Scores, B discriminant, jet  $p_T$ , number of tracks, impact parameter, and its significance and qOverP.

KEYWORDS: LHC, B-tagging, GN2,  $t\bar{t}$ ,  $Z'$ , Impact Parameter, Re-Sampling, Scores

## 1 Introduction

### 1.1 The detector

The Large Hadron Collider (LHC) at CERN is a powerful particle accelerator. It accelerates both protons and heavy ions to ultra-relativistic energies and causes them to collide. The LHC comprises four primary detectors: ATLAS, CMS, LHCb, and ALICE. ATLAS is a massive and intricate instrument designed to study the outcomes of high-energy proton-proton and heavy-ion collisions.

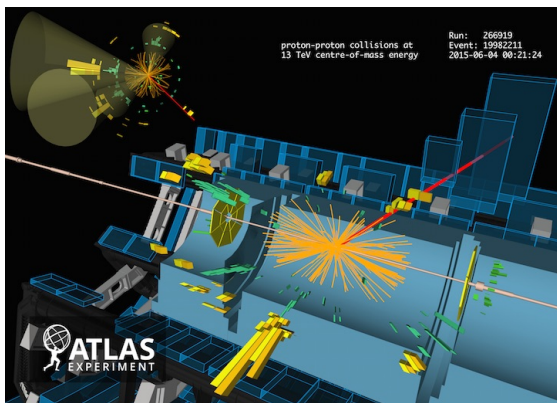


Figure 1. ATLAS Detector

In the LHC, protons are accelerated to nearly the speed of light and then directed to collide head-on at specific interaction points. These collisions release an enormous amount of energy, leading to the formation of new particles that rapidly decay into other particles. The ATLAS detector encompasses one of these collision points and is

composed of multiple layers of different types of detectors. These detectors include the Tracker, Electromagnetic Calorimeter, Hadronic Calorimeter, and Muon Spectrometer, providing valuable information about the decay products of the particles produced in the collisions. Simulation (1.4) plays a pivotal role in preparing for data acquisition at ATLAS, with a focus on simulating the ATLAS detector itself. The analysis of data derived from simulations generated by various Monte Carlo (MC) generators constitutes a fundamental step in physics analysis.

### 1.2 Jet Formation

In order to understand the data provided by ATLAS simulations, we first need to understand its underlying physics. The LHC accelerates protons to speeds close to  $c$ . During the collision, and due to the ultra-relativistic involved, the partons inside each proton interact with each other through hard scattering processes. A parton is either a quark or a gluon. The pair of interacting partons is usually composed of a quark and an anti-quark or two gluons. As a result of the collision/interaction between the two partons, two sprays of particles travelling in opposite directions are formed (the jets). The momentum of the partons is conserved. Immediately after the collision, the parton evolves into a cascade of partons, so-called a parton shower. A parton is, according to the Quantum Chromodynamics, a particle with colour charge. The partons participating in the hard scattering have huge energy and are highly unstable because of the strong force. Therefore, they decay into other particles very quickly. The parton shower evolves to the hadronization process. This means that the partons combine into hadrons. Hadrons are colourless particles composed of quarks and gluons. These particles can be neutrons, kaons, pions, protons, etc. The formation of new

<sup>a</sup>e-mail: salvadortorpes@tecnico.ulisboa.pt

particles obeys to the conversion of energy (from the parton) into mass (new particles) formula:  $E = \gamma mc^2$  where  $\gamma$  is the Lorentz factor. In the final stage the jets are composed of hadrons. Given that before the collision the transverse momentum (momentum in the perpendicular direction to the beam axis) of the system is zero the products of the collision must have a total transverse momentum equal to zero meaning that the main jets originated by each parton usually go almost in opposite directions. The jet then goes through the detector and the particles that compose it are detected by the different layers of the detector - the tracker tracks each particle's trajectory allowing the jet to be reconstructed and the calorimeters measure the energy of each particle. Each jet is composed of multiple tracks but one track can only belong to one jet. Finally, one should note that we have discussed the interaction of two partons coming from different protons. In a collision at the LHC it is possible to have more than one pair of interacting partons and therefore the number of jets produced will increase.

Here follows a scheme of the work developed in this paper: Jet Formation:

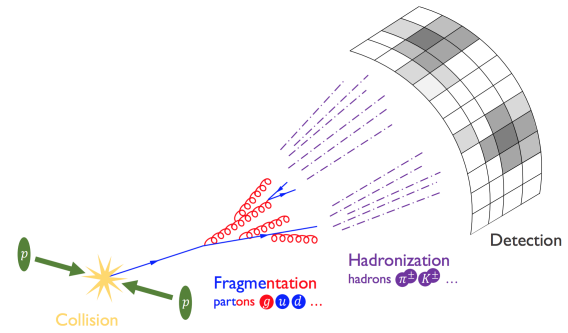
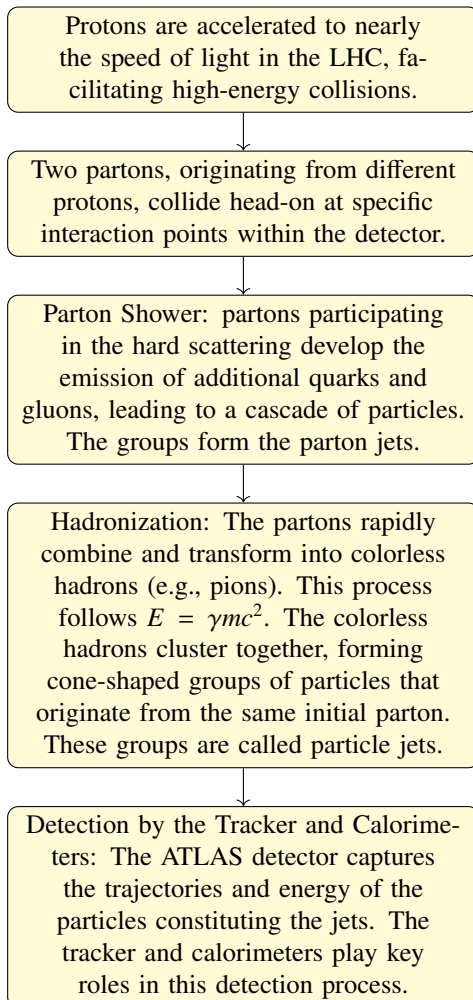


Figure 2. Jet Formation

### 1.3 Flavour-Tagging

To gain insight into the properties of jets and the particles resulting from specific parton-parton collisions (quark-antiquark or gluon-gluon), we employ a process known as flavor-tagging. Flavor-tagging involves identifying the flavor of the partons that gave rise to the jets. For instance, a jet resulting from the hadronization of a b quark is termed a b-jet. Similarly, jets originating from c-quark and u-quark collisions are referred to as c-jets and u-jets, respectively. U-jets stand for u-quark and d-quark jets and are the most prevalent. They are often referred to as light-flavor jets<sup>3</sup>. The frequency of jets is directly related to the prevalence of the parton that spawned them. Consequently, u-jets are the most common, while b-jets are the least common. The frequency of quarks decreases with their increasing mass. Remarkably, jets stemming from t quarks do not exist, as t quarks decay into b quarks before they can undergo hadronization due to their considerable mass. In addition to flavor-tagging, we employ B-tagging to identify b-jets based on their unique properties. This process enhances our understanding of the jets' origin and aids in the investigation of specific particle interactions.

**Modelo Padrão das Partículas Elementares**

	três gerações da matéria (férmions)			interações / partículas mensageiras (bósons)		
	I	II	III			
QUARKS	massa ≈2.2 MeV/c <sup>2</sup> carga 2/3 spin 1/2 <b>u</b> up	massa ≈1.28 GeV/c <sup>2</sup> carga 2/3 spin 1/2 <b>c</b> charm	massa ≈173.1 GeV/c <sup>2</sup> carga 2/3 spin 1/2 <b>t</b> top	0 0 1 <b>g</b> glúon	massa ≈124.37 GeV/c <sup>2</sup> 0 0 <b>H</b> higgs	
	massa ≈4.7 MeV/c <sup>2</sup> carga -1/3 spin 1/2 <b>d</b> down	massa ≈96 MeV/c <sup>2</sup> carga -1/3 spin 1/2 <b>s</b> strange	massa ≈4.18 GeV/c <sup>2</sup> carga -1/3 spin 1/2 <b>b</b> bottom	0 0 1 <b>γ</b> fóton	BÓSONS ESCALARES	
	massa ≈0.511 MeV/c <sup>2</sup> carga -1 spin 1/2 <b>e</b> elétron	massa ≈105.66 MeV/c <sup>2</sup> carga -1 spin 1/2 <b>μ</b> múon	massa ≈1.778 GeV/c <sup>2</sup> carga -1 spin 1/2 <b>τ</b> tau	0 1 1 <b>Z</b> bóson Z		
	massa ≈0.0 eV/c <sup>2</sup> carga 0 spin 1/2 <b>ν<sub>e</sub></b> neutrino do elétron	massa ≈0.17 MeV/c <sup>2</sup> carga 0 spin 1/2 <b>ν<sub>μ</sub></b> neutrino do múon	massa ≈1.82 MeV/c <sup>2</sup> carga 0 spin 1/2 <b>ν<sub>τ</sub></b> neutrino do tau	±1 ±1 1 <b>W</b> bóson W		

**BÓSONS DE GAUGE** (Bósons Vetoriais)

Figure 3. Standard Model of Elementary Particles

B-jets are characterised by a structure that exhibits one particular feature that is not present in other jets: a measurable displaced secondary vertex. This secondary vertex allows us to identify b-jets through the properties of this vertex and impact parameter variables ( $d_0$  and  $z_0$ ).

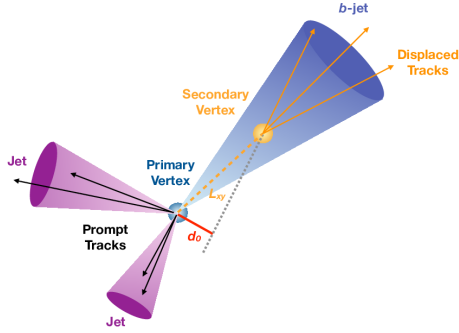


Figure 4. B-jet Structure

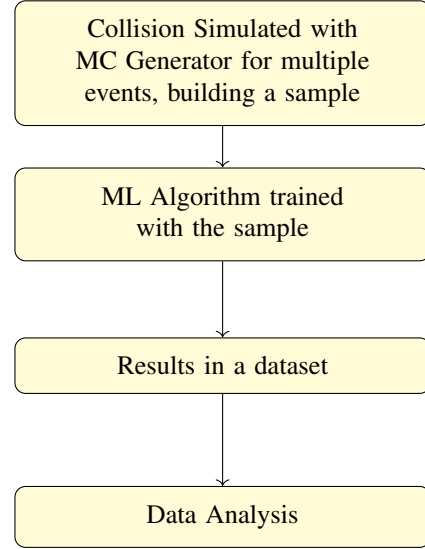
#### 1.4 Simulation and Monte Carlo Generators

The collision process discussed in Section 1.2 is simulated using Monte Carlo (MC) generators, specifically Pythia8 ([1]) and Herwig7 ([2]). These generators are employed to simulate both the collision process and the subsequent hadronization process. While Pythia8 is widely used, this study aims to compare it with the less common Herwig7. The outcome of the simulation is a sample resembling the data obtained from real measurements at the detector. Since it is a simulation, we possess knowledge of the jet flavors, as we know the flavors of the partons that originated them. This sample comprises an extensive number of events, each representing a particular collision type. Each event provides the sample with information about its jets and their respective properties. Typically, this information is organized into two distinct types of variables: jet variables, describing the jets as a whole, and track variables, which vary from track to track within the jet. The simulation can be performed with various types of events. In our study, we will utilize  $t\bar{t}$  and  $Z'$ . The  $t\bar{t}$  event simulates the collision of a  $t$  quark and anti-quark. These events have a higher likelihood of producing b-jets, as top quarks, being significantly heavier, almost always decay into b-quarks before undergoing hadronization. Consequently, the formation of b-jets in low  $p_T$  ranges is highly probable in the  $t\bar{t}$  sample.  $Z'$  is a hypothetical gauge boson that arises from extensions of the Standard Model of Elementary Particles. It has been generated with a mass equal to 700 GeV and it is used in order to study the B-tagging performance algorithms at large transverse momentum ranges.

#### 1.5 Machine Learning

Once the collision process is simulated, Machine Learning (ML) algorithms are employed for flavor-tagging of

the jets. The primary objective is to train these algorithms on simulated datasets to enhance their tagging capabilities, subsequently enabling their application to real data for jet flavor identification. One of the most widely used ML algorithms for B-tagging is RNNIP (Recurrent Neural Network Impact Parameter), which serves as a reference for comparison with the GN2 algorithm, the focal point of this paper's development. The GN2 (2nd generation Graphical Neural Learning) algorithm, being novel, garners significant attention in this study.



For each jet in the sample, the algorithm generates three scores: the probability of the jet being a b-jet, the probability of it being a c-jet, and the probability of it being a u-jet. To study the B-tagging algorithm, an analysis is conducted to investigate how its scores vary concerning different variables, such as jet transverse momentum. The ideal scenario is to achieve a distinct separation between the three types of jets, signifying the algorithm's ability to differentiate and consequently identify the jets flavors. In the ideal case, the algorithm would output a b-score of 1 for b-jets, a c-score of 1 for c-jets, and a u-score of 1 for u-jets. However, due to the strikingly similar properties of these jets and the similarities in the decay products of different quarks, it proves to be quite challenging to differentiate between the three types of jets accurately. Hence, the algorithm's scores will not precisely reach 1 for the correct jets.

#### 1.6 Discriminant

Based on the scores provided by a specific algorithm for a simulated sample, it is possible to calculate a discriminant that will help us understand how well the algorithm is able to differentiate between the different types of jets. The B-discriminant of a jet is calculated using the following formula:

$$D_b = \log \left( \frac{P_b}{f_c \times P_c + f_u \times P_u} \right) \quad (1)$$

Where  $P_b$  is the b-score of the jet,  $P_c$  is the c-score of the jet,  $P_u$  is the u-score of the jet and  $f_c$  and  $f_u$  are the fractions of c-jets and u-jets in the sample respectively. For a

given jet, the bigger the B-discriminant is, the more likely it is for the algorithm to correctly identify the jet as a b-jet. The C-discriminant is given by:

$$D_c = \log\left(\frac{P_c}{f_b \times P_b + f_u \times P_u}\right) \quad (2)$$

Where  $f_b$  is the fraction of b-jets in the sample.

## 1.7 Datasets Used

This paper will analyze datasets coming from the GN2 algorithm. These datasets come from two different samples ( $t\bar{t}$  and  $Z'$ ) and two different MC generators (Pythia8 and Herwig7):

ML Tagger	MC Generator (Simulates the Sample)	Events on the Sample
GN2	Pythia	$Z'$ prime
		$t\bar{t}$
	Herwig	$Z'$ prime
		$t\bar{t}$

The results were obtained via code written in Python using the PUMA and MATPLOTLIB libraries. Generally, each histogram contains 1 000 000 events for statistical purposes.

## 2 Transverse Momentum

In order to confirm the nature of both the samples used, we plotted the transverse momentum of the jets. Firstly, for the  $t\bar{t}$  samples:

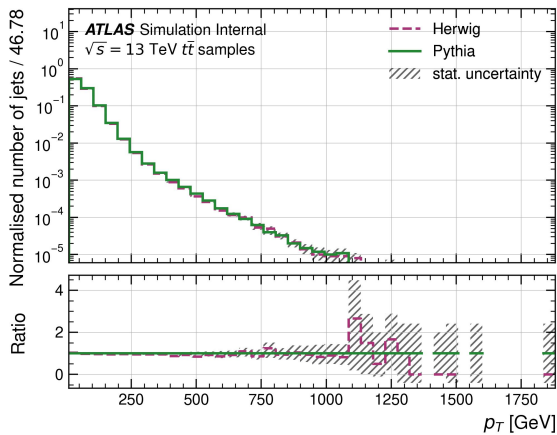


**Figure 5.** The transverse momentum,  $p_T$ , distribution for  $t\bar{t}$  event sample generated by Pythia and Herwig. All flavours summed.

$t\bar{t}$  samples have low  $p_T$  values as expected.

For the  $Z'$  samples:

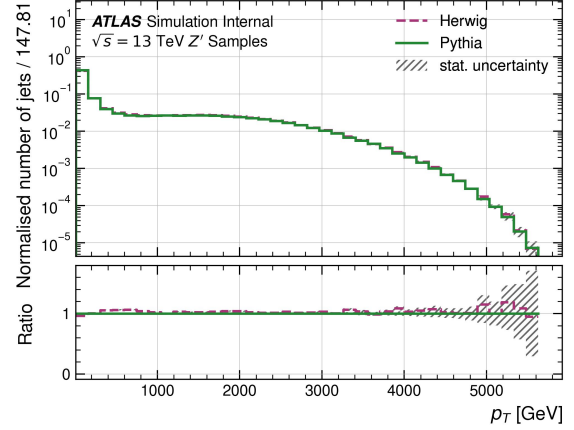


**Figure 6.** The transverse momentum,  $p_T$ , distribution for  $Z'$  event sample generated by Pythia and Herwig. All flavours summed.

$Z'$  samples have higher  $p_T$  values than  $t\bar{t}$  samples as expected. In both cases, the Herwig and Pythia data are very similar.

## 3 Track Variables

Focusing on the track variables, we plotted histograms for the following variables:

### 3.1 Charge over Momentum

The electric charge of the particle over its momentum is expected to be symmetrically distributed around 0 and have no bins at 0 because electrically neutral particles are not detected - the Inner Tracker of ATLAS only detects charged particles. The results for both samples are:

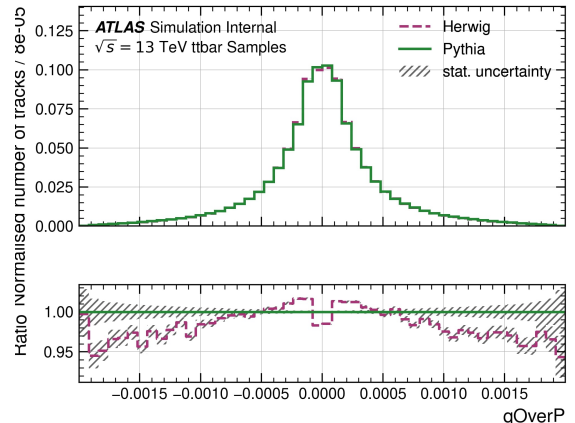


**Figure 7.** qOverP for  $t\bar{t}$  sample all flavours summed

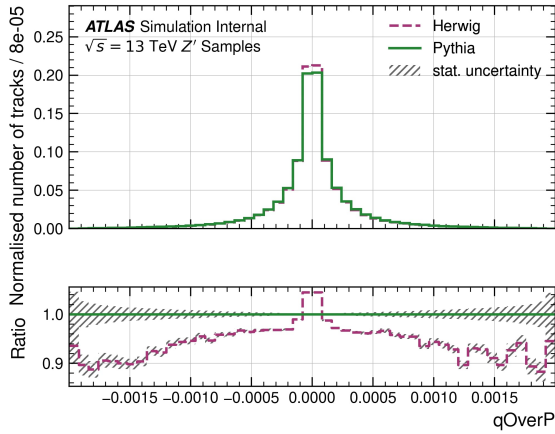


Figure 8. qOverP for Z' sample all flavours summed

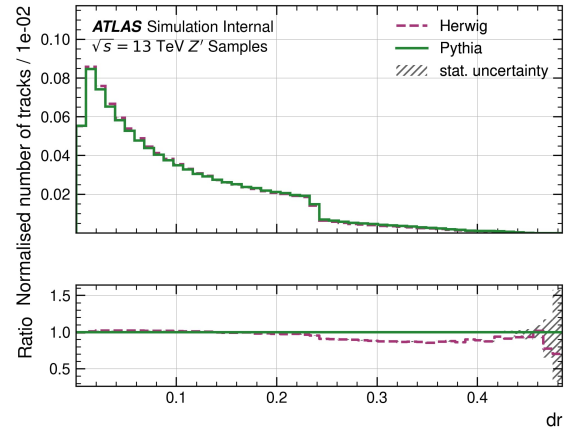


Figure 10. dr for Z' sample all flavours summed

As expected, both distributions are symmetrical because it is equally likely for a detected charged particle to have charge  $q$  or  $-q$ . Differences between Herwig and Pythia up to 10% can be observed - they are more significant in the Z' sample. The data is more spread out across the bins for the  $t\bar{t}$  sample which results in a lower peak at 0: 10 % of the data is at 0 for the  $t\bar{t}$  sample and 20 % of the data is at 0 for the Z' sample.

The density of tracks decreases as  $dr$  increases. Notice a displacement around 0,24 only present in the Z' Sample. Pythia and Herwig values differ above this point. Figures 9 and 10 were also plotted in logarithmic scale and the results are in appendix A figures 32 and 33.

### 3.2 Distance from the Jet Axis

The  $dr$  variable is the distance between the track and the jet axis. The results for both samples are:

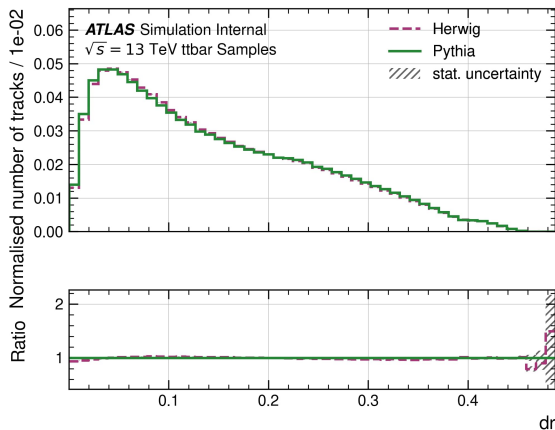


Figure 9. dr for  $t\bar{t}$  sample all flavours summed

### 3.3 Impact Parameter

The impact parameter is the distance between the track and the primary vertex. The plots for  $d0$  are as follows:

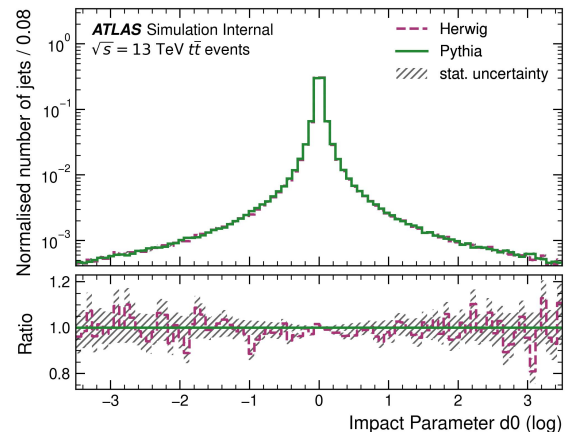
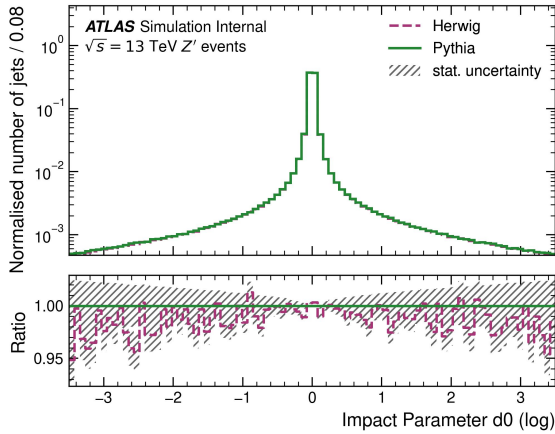


Figure 11. The impact parameter,  $d0$ , distribution for the  $t\bar{t}$  sample. All flavours summed.



**Figure 12.** The impact parameter,  $d_0$ , distribution for the  $Z'$  sample. All flavours summed.

As expected, in both samples (figures 11 and 12), the amount of tracks decreases as the impact parameter increases - the further away from the leading track, the least tracks are found. In addition, no differences between Herwig and Pythia can be observed outside the statistical uncertainty.

### 3.4 Impact Parameter Significance

The impact parameter significance is the impact parameter divided by its uncertainty. The plots for this variable are as follows:

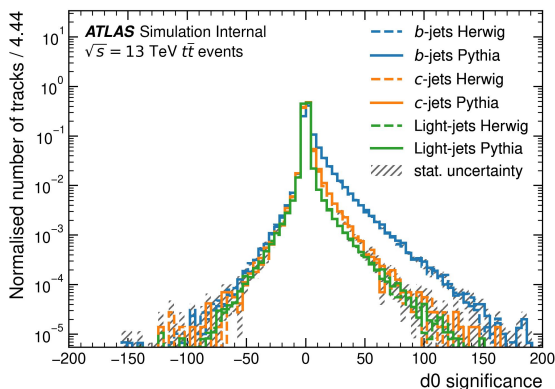


**Figure 13.** The  $d_0$  significance distribution for the  $t\bar{t}$  sample. All flavours summed.

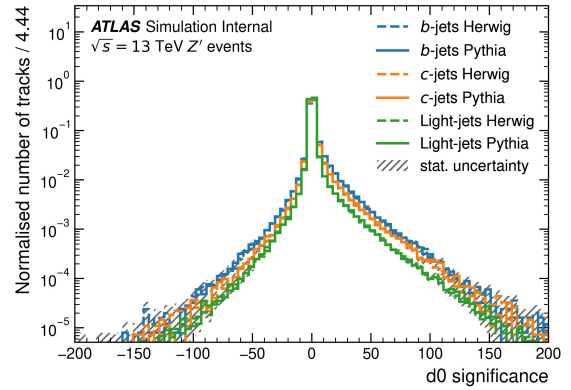


**Figure 14.** The  $d_0$  significance distribution for the  $Z'$  sample. All flavours summed.

### 3.5 TruthOriginLabel

The TruthOriginLabel concerns the generated parton that will originate the jet.

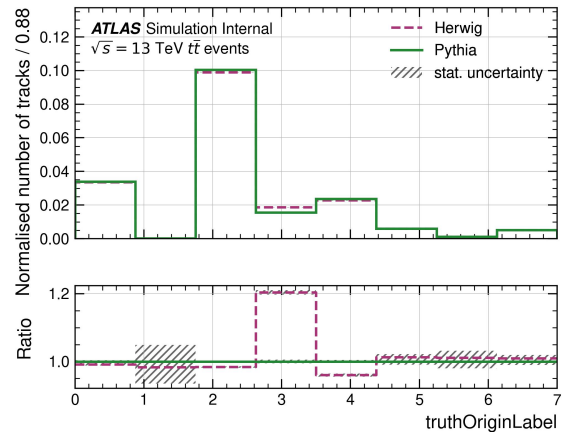


**Figure 15.** TruthOriginLabel for  $t\bar{t}$  sample.

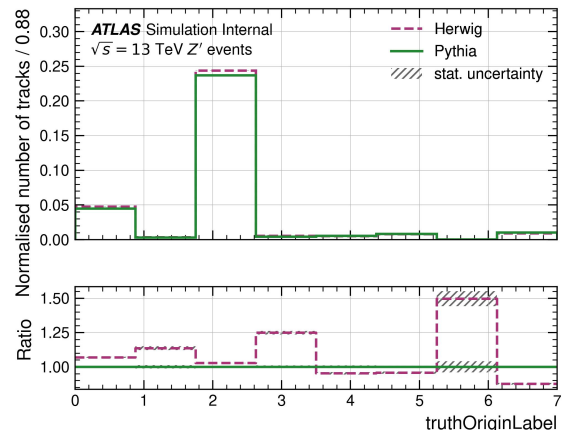


**Figure 16.** TruthOriginLabel for  $Z'$  sample.

## 4 Number of Tracks

In order to study the number of tracks of each jet flavour and also its variation with jet  $p_T$ , the following histograms are plotted:

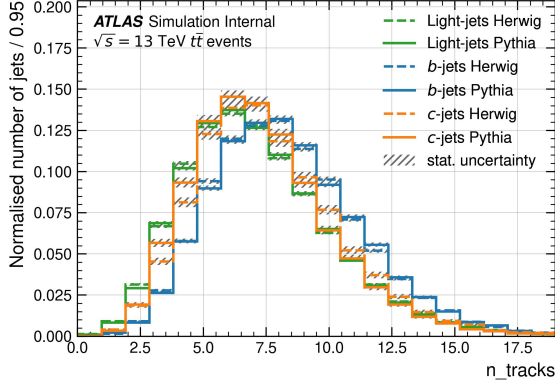


**Figure 17.** The track multiplicity distribution for jets in the  $t\bar{t}$  sample. All flavours.

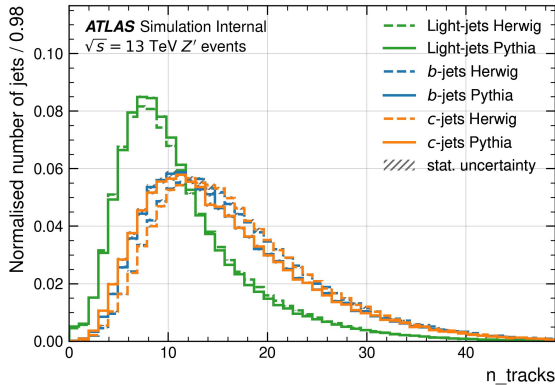


**Figure 18.** The track multiplicity distribution for jets in the  $Z'$  sample. All flavours.

For the  $t\bar{t}$  sample (figure 17), the number of tracks is approximately the same for u- and c-jets with the most probable value at 6 tracks per jet. The b-jet distribution is shifted towards larger multiplicities. On the other hand, for the  $Z'$  sample (figure 18), the number of tracks is higher for b-jets and c-jets than for u-jets and it peaks at 8 tracks per jet for light jets and 11 tracks per jet for b-jets and c-jets. In both cases the distributions are very similar: increase rapidly until the peak and then decrease slowly.

In order to study the differences between Herwig and Pythia, histograms with this variable were plotted for all flavours summed:

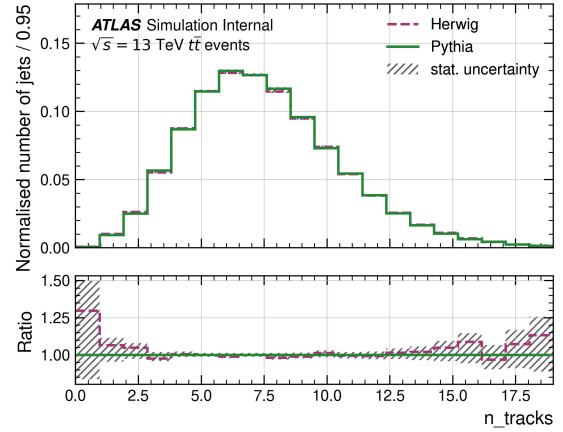


**Figure 19.** The track multiplicity distribution for jets in the  $t\bar{t}$  sample. All flavours summed.

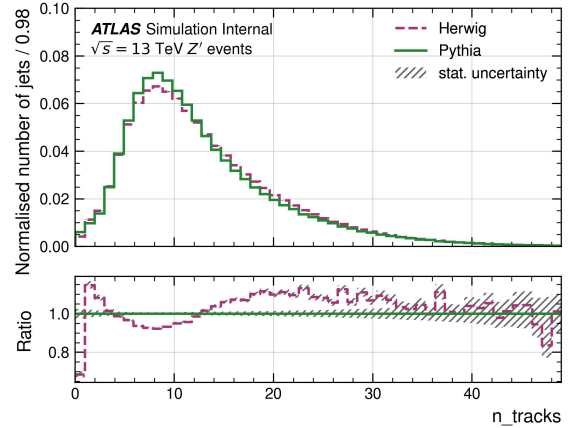


**Figure 20.** The track multiplicity distribution for jets in the  $Z'$  sample. All flavours summed.

For the  $t\bar{t}$  sample (figure 19), the number of tracks is approximately the same for both generators. However, major differences can be observed in figure 20 for the  $Z'$  sample. Differences between Herwig and Pythia can be observed up to 10%.

## 5 Score Variables

In order to study the score variables, we plotted histograms for each one of the scores. The complete data with histograms separated by flavour and type of jet is available in the appendix 2, 3 and 4. Note that, in the following histograms we can observe, in the y-axis, the probability of the GN2 algorithm to associate a jet as a b-jet, c-jet, or u-jet with the b, c, or u score in the x-axis. The ratio panels show the ratio between the Herwig and Pythia histograms. The ratio is calculated by dividing the Herwig histogram by the Pythia data in order to compare the two generators.

## 5.1 $t\bar{t}$ Samples

In the following samples, we can see histograms for three different scores in the  $t\bar{t}$  samples: GN2v00\_pu, GN2v00\_pc and GN2v00\_pb.

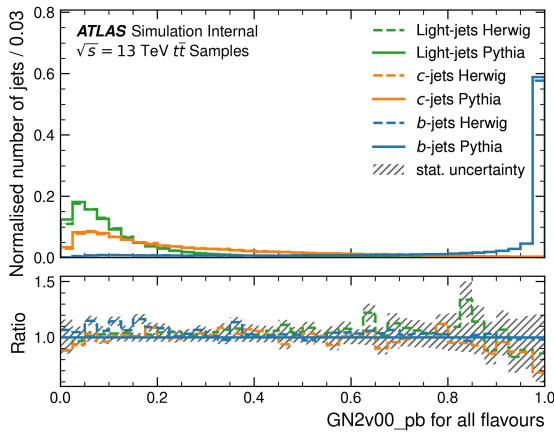


**Figure 21.** Normalised number of jets as a function of score GN2v00\_pb for the  $t\bar{t}$  sample. All flavours.

As expected, b jets are very likely to have a  $\approx 1$  b score and close to 0 c and u scores.

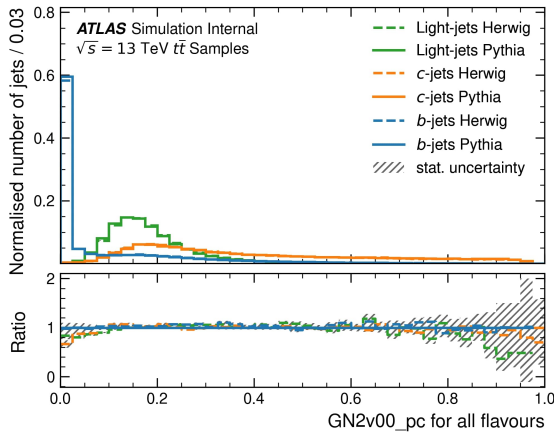


**Figure 22.** Normalised number of jets as a function of score GN2v00\_pc for the  $t\bar{t}$  sample. All flavours.

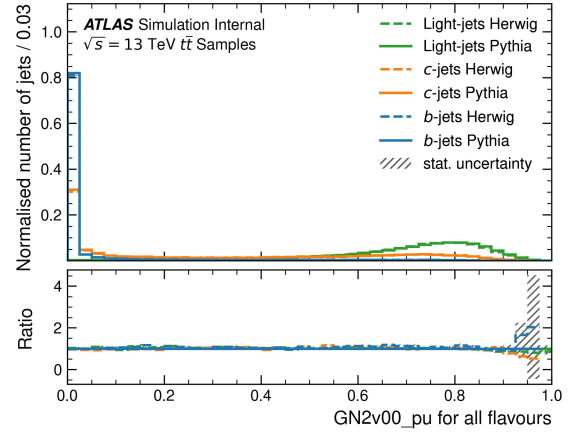


**Figure 23.** Normalised number of jets as a function of score GN2v00\_pu for the  $t\bar{t}$  sample. All flavours.

The c and u scores are very low in both cases for b jets. However c jets and u jets are never likely to have a  $\approx 1$  c or u score respectively. This is due to the fact that we are working with a b-tagging algorithm therefore its main goal is to identify b jets. Herwig and Pythia differences are not very noticeable in any of the three scores since the ratios show no differences within the statistical uncertainty.

## 5.2 $Z'$ Samples

Here are the same results for the  $Z'$  samples.

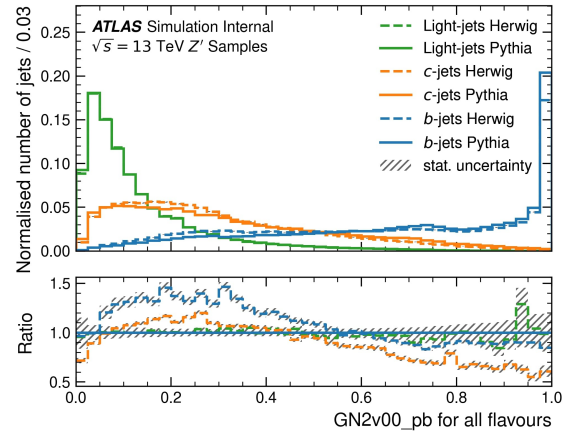


**Figure 24.** Normalised number of jets as a function of score GN2v00\_pb for the  $Z'$  sample. All flavours.

As expected and, similarly to the  $t\bar{t}$  samples, b jets are very likely to have a  $\approx 1$  b score and low c and u scores. However, apart from what can be observed in figure 21, in figure 24 there is an  $\approx 50\%$  difference between Herwig and Pythia for low scores in b jets and for high scores in c jets. There is also an  $\approx 20\%$  difference between Herwig and Pythia for low scores in c jets.

In figure 21, score b has 60 % of the data with a score of 1 for b jets and in figure 24 score b only has 20 % of the data with a score of 1 for b jets.

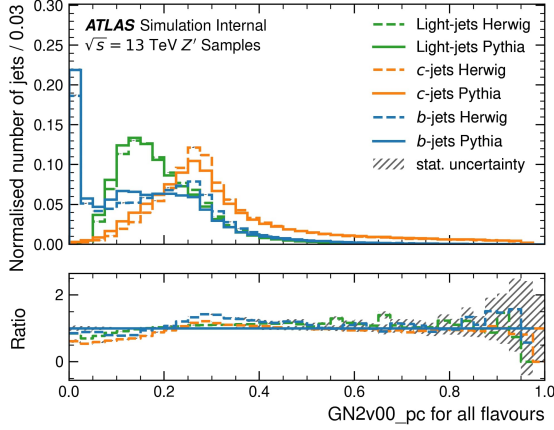


**Figure 25.** Normalised number of jets as a function of score GN2v00\_pc for the  $Z'$  sample. All flavours.

In figure 25 score c is very low for b jets, as expected, and oscillation between 0.1 and 0.4 for c jets and u jets can be observed. The algorithm behaves differently than in the  $t\bar{t}$  samples in the figure 22: the three jets have lower probabilities at their peak but the most significant difference is in the b jets - for the  $t\bar{t}$  samples, b jets have a c score of 0 for 60 % of the data and for the  $Z'$  samples, b jets have a c score of 0 for 22 % of the data. Lastly, for low scores, Herwig and Pythia show < 50 % difference for the three flavors for c scores smaller than 0.4.

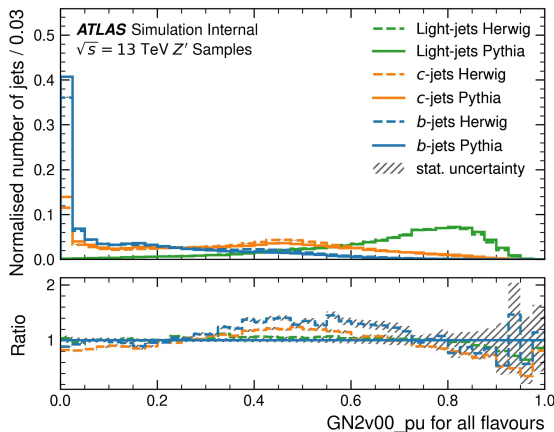


**Figure 26.** Normalised number of jets as a function of score GN2v00\_pu for the  $Z'$  sample. All flavours.

For the u score, b jets peak around 0 and c and u jets oscillate between 0.4 and 0.85. Herwig and Pythia differences are only noticeable for b and c jets for scores bigger than 0.3 and smaller than 0.7. Once more, if we compare 26 with 23, we can see that the algorithm behaves differently in the  $Z'$  samples than in the  $t\bar{t}$  samples: for the b

jets, u score is 0 for 80 % of the data in the  $t\bar{t}$  samples and for 40 % of the data in the  $Z'$  samples.

### 5.3 $t\bar{t}$ vs $Z'$ Samples

Comparing the results in sections 5.1 and 5.2, we can see that the algorithm behaves differently in the  $t\bar{t}$  samples and in the  $Z'$  samples. For the  $Z'$  samples, there is a tendency to have more dispersion in the scores than in the  $t\bar{t}$  samples - that is why the histograms in the  $Z'$  samples have more oscillation and the higher peaks of each score, even though located in the same place, are lower than in the  $Z'$  samples. Peaks of  $Z'$  samples are less intense because they have higher  $p_T$  and B Tagging algorithms are not as exact for high  $p_T$  as they are for lower  $p_T$  ( $t\bar{t}$ ) - the variables that allow the algorithm to identify b jets lose significance as the jet  $p_T$  increases.

## 6 Score Variables Variation with $p_T$

In order to confirm if the scores vary with the transverse momentum of the jets, we plotted 2D Histograms for the three scores Herwig and Pythia for the  $t\bar{t}$  and  $Z'$  samples. The histograms are available in the appendix.

For fixed values of  $p_T$ , the scores have similar distributions to those observed in section 5 for all cases. For fixed values of score, the counts of each bin decreases as  $p_T$  increases for both  $t\bar{t}$  and  $Z'$  samples: this decrease is much more evident in the  $t\bar{t}$  samples because their  $p_T$  values are lower than the  $Z'$  samples as it can be seen in figures 5 and 6.

## 7 Score Variables Variation with each other

During our investigation of the GN2 algorithm, we came across the need to study the variation of the scores with each other. We suspected that both c and b scores would express repeated behaviour when plotted against the u score. 2D histograms were plotted for both c and b scores against the u score for the  $t\bar{t}$  and  $Z'$  samples. In order to observe the behaviour we intended to study, two types of techniques were used:

1. 'Tendential Lines': these are curves fitted to the points of the histogram with the highest counts. They are used to observe the behaviour of the scores in the region where they have the highest counts. They have no physical meaning and they are present only to help us understand the behaviour of the scores.
2. Weighted Mean: for each x bin of the histogram, we calculated the weighted mean of the y bins according to the number of counts of each bin. This allows us to observe the region where the scores have the highest counts.

We considered both Herwig and Pythia samples for the  $t\bar{t}$  and  $Z'$  events. The results are in the appendix B. As we can see, there is a behaviour common to both generator and events: for low  $u$  scores, the  $b$  score is higher than the  $c$  score, and for high  $u$  scores, the  $c$  score is higher than the  $b$  score. This behaviour indicates that the algorithm is more likely to identify a jet as a  $b$  jet if it is highly unlikely for it to be an  $u$ -jet.

This behaviour can be further observed if we plot the sum of the  $c$  and  $b$  scores against the  $u$  score and then overwrite the histogram with the 'tendential lines' and the weighted mean for both  $c$  and  $b$  scores:

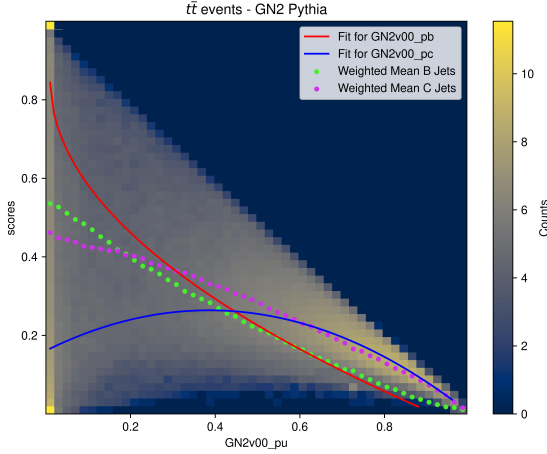


**Figure 27.** Scores  $c$  and  $b$  against  $u$  for  $t\bar{t}$ . Sample: Pythia.

The equivalent plots for  $t\bar{t}$  Herwig,  $Z'$  Pythia, and  $Z'$  Herwig are in the appendix B.

Analyzing the images 35, 36, 27 and 34, we can see that the scores have similar behaviour in all cases to the one described earlier.

## 8 B Discriminant

In order to study the GN2 algorithm and its ability to differentiate between the different types of jets, we plotted 1D and 2D histograms for the  $b$  discriminant. To compute the  $b$  discriminant, we considered  $f_c = 0.018$ . Here follow the results for both  $Z'$  and  $t\bar{t}$  samples:

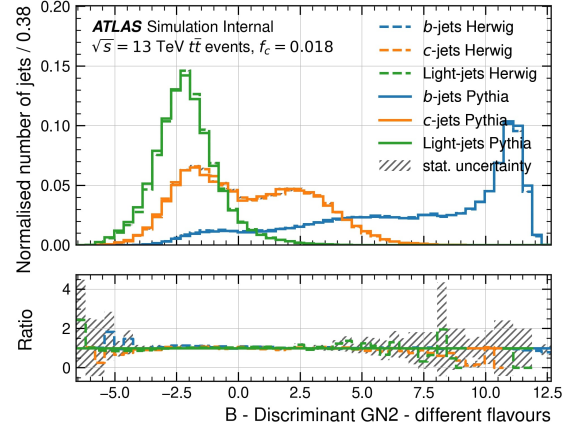


**Figure 28.** Normalised number of jets as a function of the GN2 B-Discriminant for the  $t\bar{t}$  sample. All flavours.

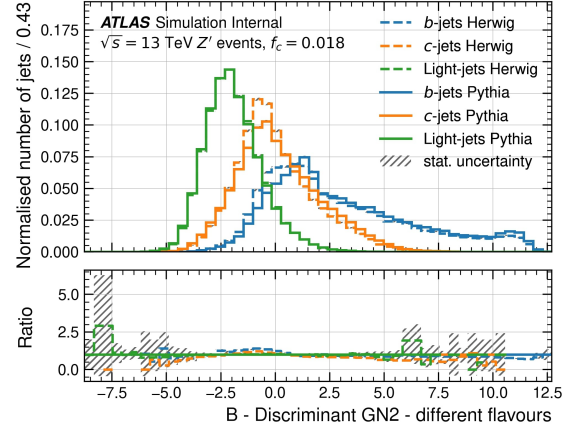


**Figure 29.** Normalised number of jets as a function of the GN2 B-Discriminant for the  $Z'$  sample. All flavours.

In figure 28, Herwig and Pythia data only differ within the statistical uncertainty. Nonetheless, the  $b$  discriminant has higher values for  $b$  jets, peaking around 10.0. For light jets, it only has one peak around -2.5 and for  $c$  jets, it has two peaks: one around -2.5 and another around 2.5. As it is expected,  $b$  jets have, in general, higher B-Discriminant values than  $c$ -jets and  $u$ -jets.

In the  $Z'$  samples, however, the B-Discriminant does not have such a clear separation between  $b$ -jets and  $c$ - and  $u$ -jets as it did in the  $t\bar{t}$  samples. As we can see in figure 29, the B-Discriminant has two peaks for  $b$  jets: one around 11.0 and another around 2.0. The first peak is more intense than the second one and it is located close to the peaks of the  $b$  discriminant for  $c$ - and  $u$ -jets, respectively at -1.5 and -2.5.

## 9 Re-sampling

During our investigation, it became important to consider re-sampled events in order to better understand the results

obtained. Re-sampling is a technique that ensures equal number of the three jet flavours in each bin of  $p_T$ .<sup>1</sup> Usually, the b jets are the least common meaning each bin's number of c and u jets is reduced to the number of b jets. No major differences were observed in the results obtained with re-sampled events. For example, here follows the GN2 b-score for re-sampled events in the  $Z'$  sample:

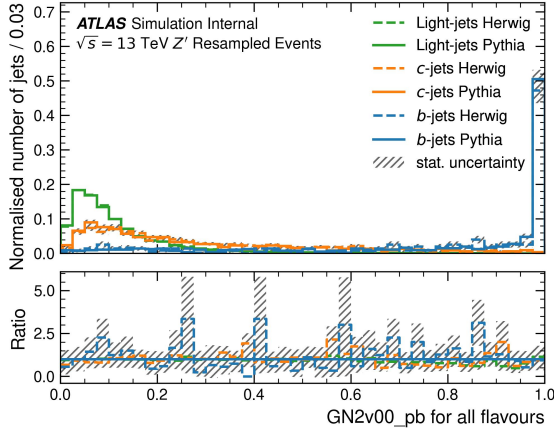


**Figure 30.** Score GN2v00\_pb for  $Z'$  Re-sampled events

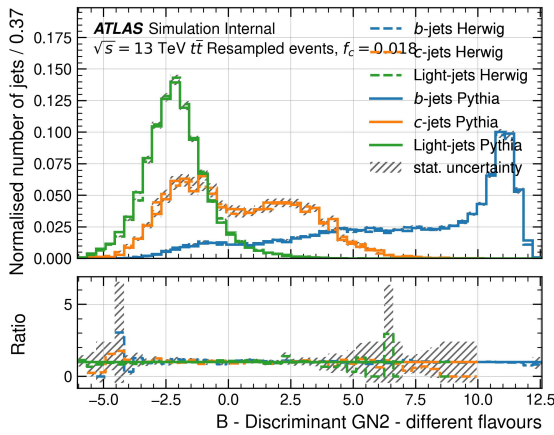


**Figure 31.** B-Discriminant for  $t\bar{t}$  Re-sampled events

The results on figure 31 are very similar to the ones obtained in 24 for the  $Z'$  samples. However, it should be noted that when Re-Sampling, the differences between Herwig and Pythia become non-significant for  $p_T$ , scores and B-discriminant plots. In  $t\bar{t}$  samples the same effect can be observed.

## 10 Results and Conclusions

In this paper, our primary objective was to investigate the GN2 algorithm's performance. Regarding b-tagging, we have reached the conclusion that this algorithm yields remarkable results for identifying b-jets, regardless of whether they are in high ( $Z'$ ) or low ( $t\bar{t}$ )  $p_T$  ranges. It is

important to note that when comparing the performance of the algorithm across two Monte Carlo generators, Herwig7 and Pythia8, we observed more pronounced differences in  $Z'$  samples compared to  $t\bar{t}$  samples.

However, it's worth highlighting that when we resampled the datasets to ensure a more balanced representation of different jet flavors across multiple eta and  $p_T$  bins, the disparities between Herwig and Pythia disappeared. This adjustment helped to create a fairer comparison between the two generators.

Lastly, our investigation also delved into a specific behavior of the GN2 algorithm concerning the relationship between its three scores. We consistently observed that jets with low u-scores tended to exhibit higher b-scores than c-scores, while in jets with higher u-scores, the opposite pattern emerged. This insight could eventually provide valuable information about the algorithm's behavior in different contexts.

## Acknowledgements

Thank you Helena for all the work we have done together. It was a pleasure working with you.

## References

- [1] T.S. et al., Comput. Phys. Commun. **191** (2015), arXiv:1410.3012 [hep-ph]
- [2] M.B. et al., Eur. Phys. J. C **58** (2008), arXiv:0803.0883 [hep-ph]

<sup>1</sup>and pseudorapidity  $\eta$ . Results not shown in this paper though.

### A $dr$ in Logarithmic Scale

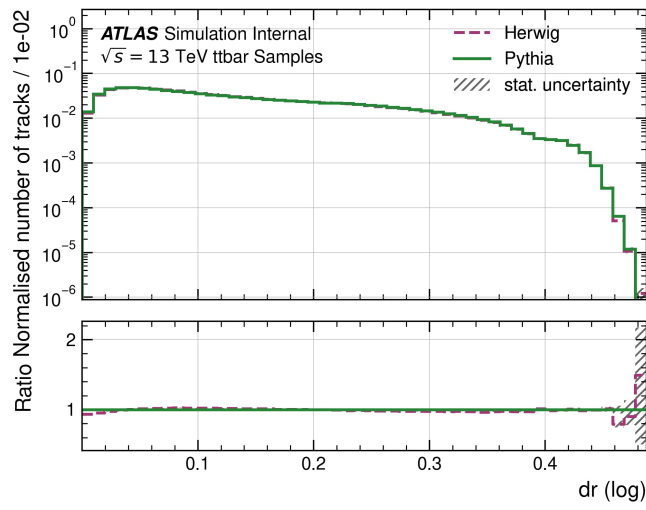


Figure 32.  $dr$  for  $t\bar{t}$  sample all flavours summed

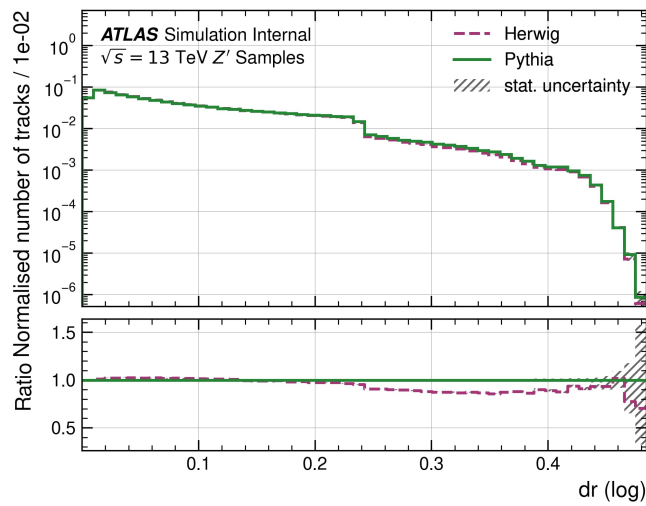


Figure 33.  $dr$  for  $Z'$  sample all flavours summed

### B Score Variables Variation with each other

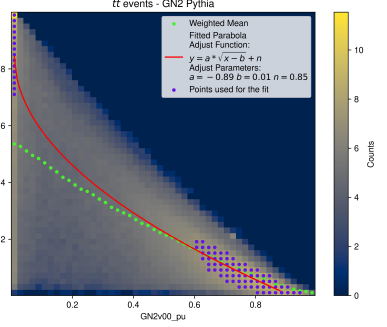
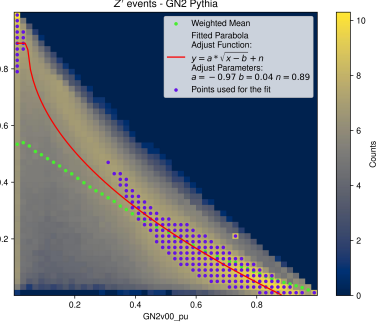
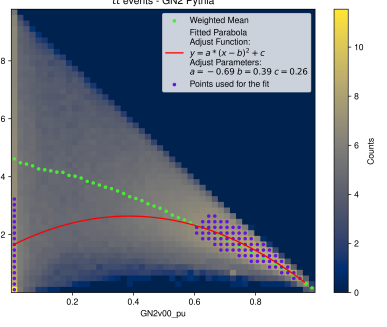
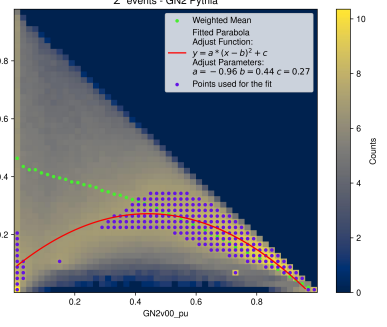
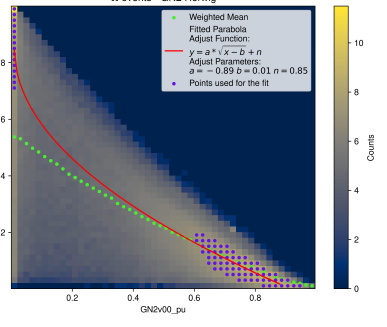
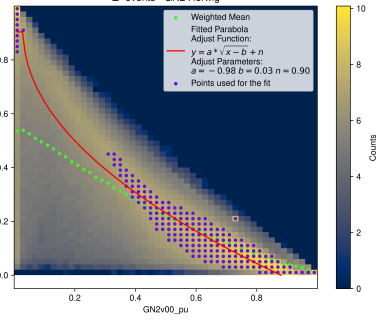
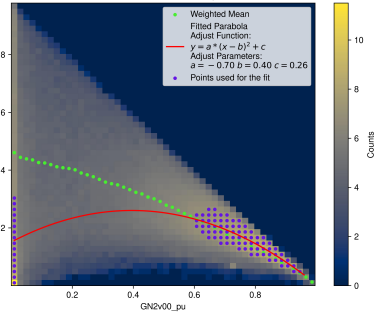
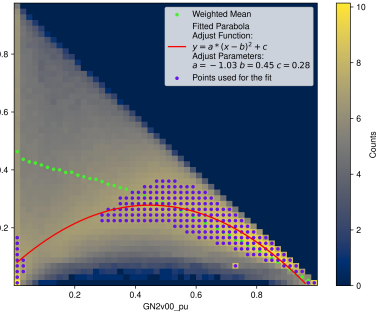
Description	$t\bar{t}$ Events	$Z'$ Events
Pythia score b and u		
Pythia score c and u		
Herwig score b and u		
Herwig score c and u		

Table 1. Score Variables Variation with each other

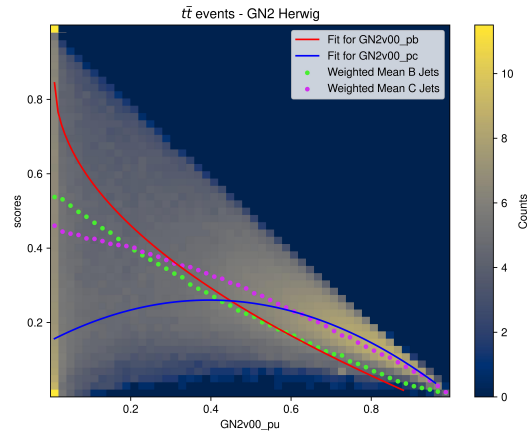


Figure 34. Score c and b against u for  $t\bar{t}$  sample Herwig

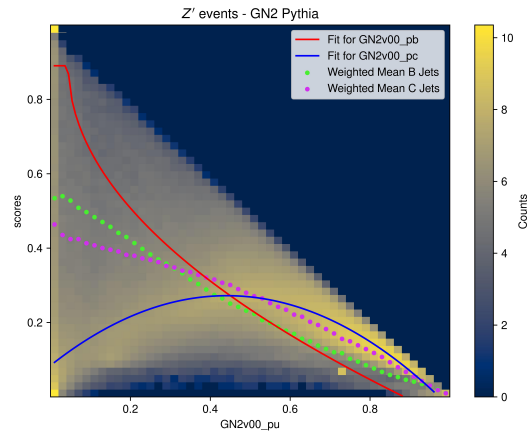


Figure 35. Score c and b against u for  $Z'$  sample Pythia

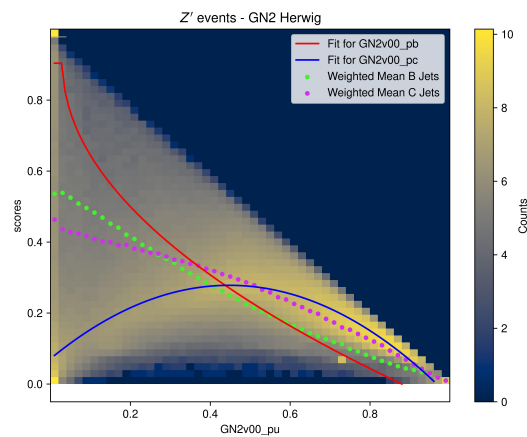
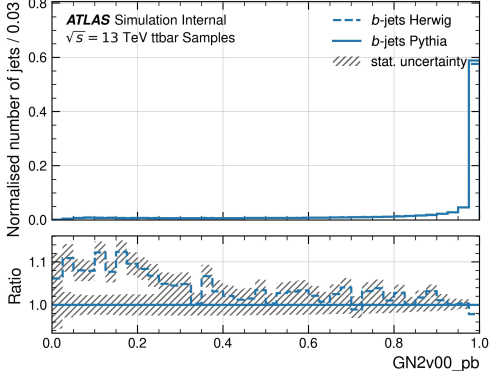
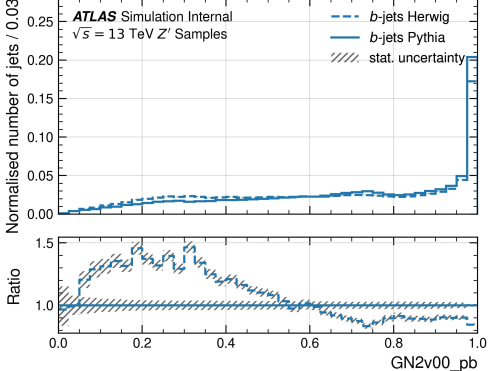
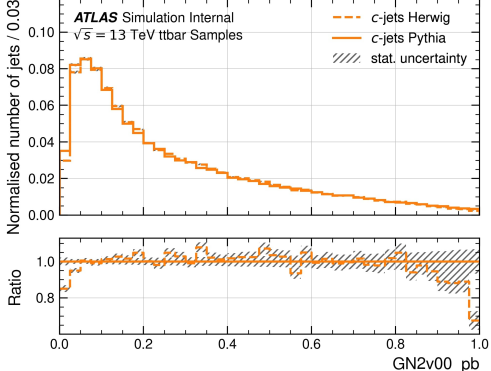
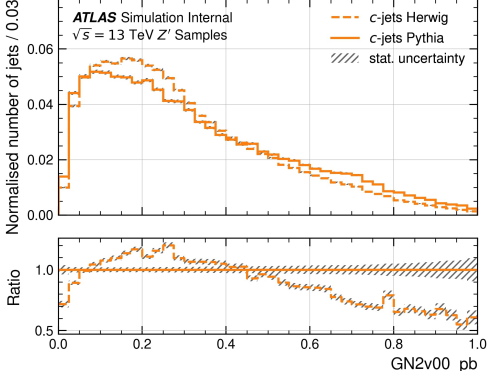
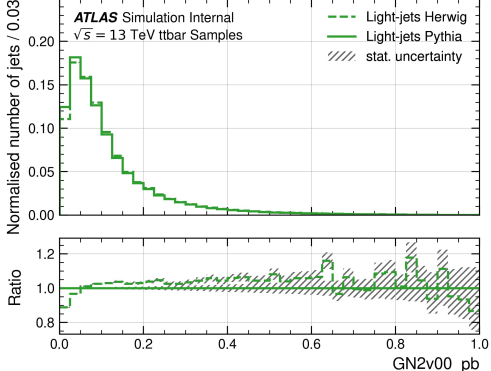
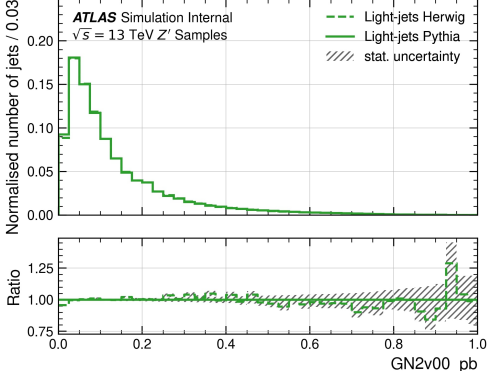


Figure 36. Score c and b against u for  $Z'$  sample Herwig

### C Score Histograms

Description	$t\bar{t}$ Events	$Z'$ Events
<p>Herwig and Pythia b jets score b GN2v00_pb</p>		
<p>Herwig and Pythia c jets score b GN2v00_pb</p>		
<p>Herwig and Pythia u jets score b GN2v00_pb</p>		

**Table 2.** Scores Histograms for GN2v00\_pb

by

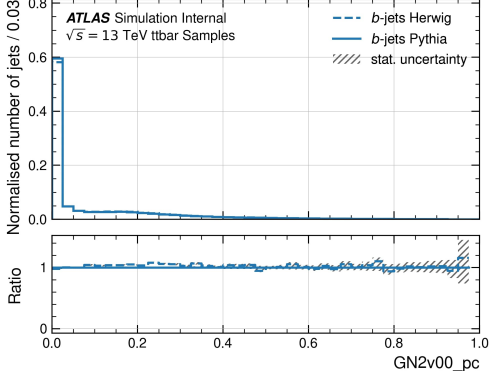
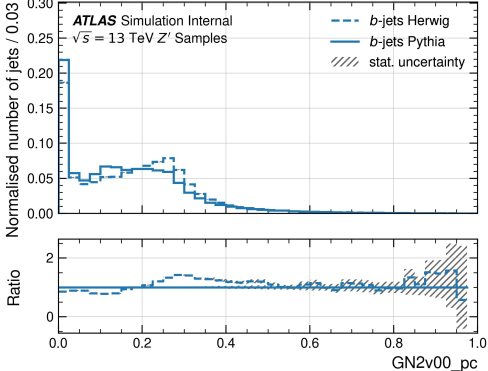
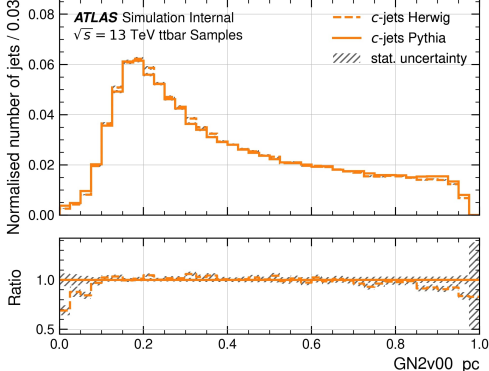
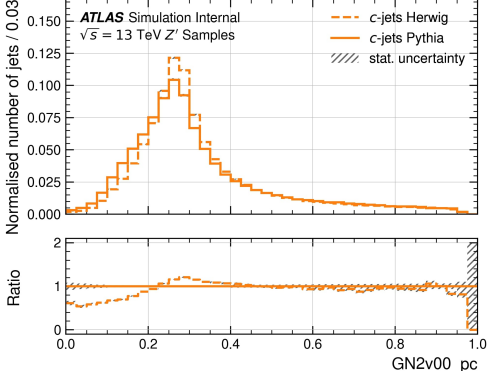
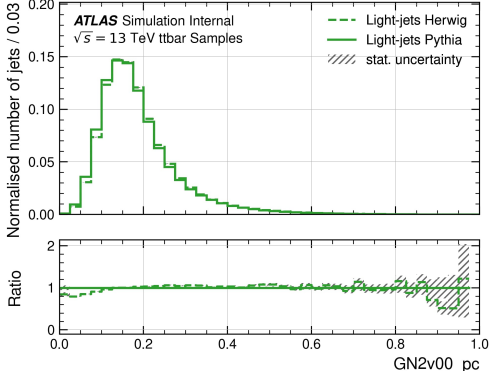
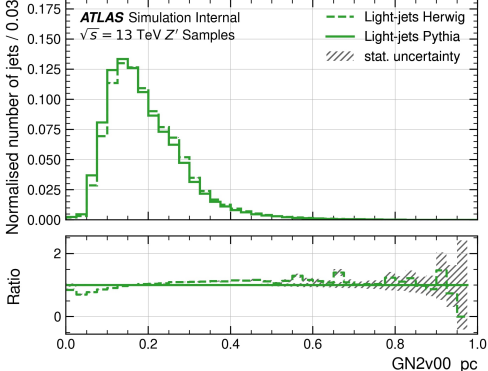
Description	$t\bar{t}$ Events	$Z'$ Events
<p>Herwig and Pythia b jets score c GN2v00_pc</p>		
<p>Herwig and Pythia c jets score c GN2v00_pc</p>		
<p>Herwig and Pythia u jets score c GN2v00_pc</p>		

Table 3. Scores Histograms for GN2v00\_pc

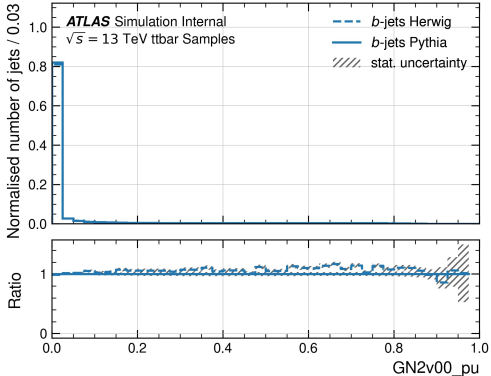
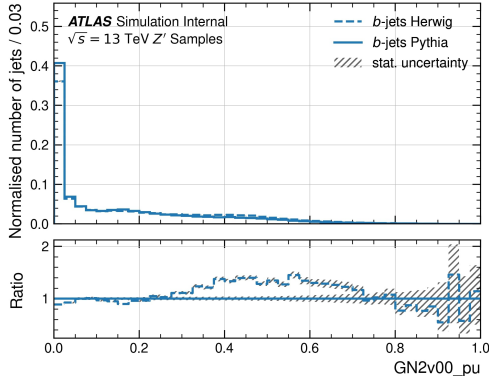
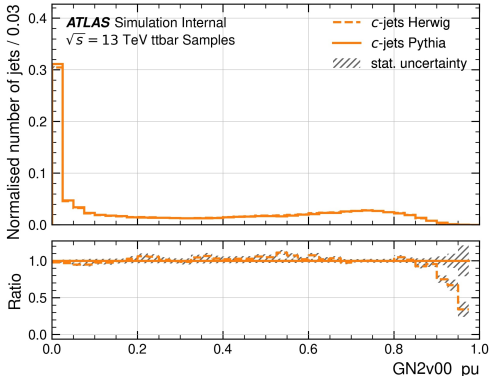
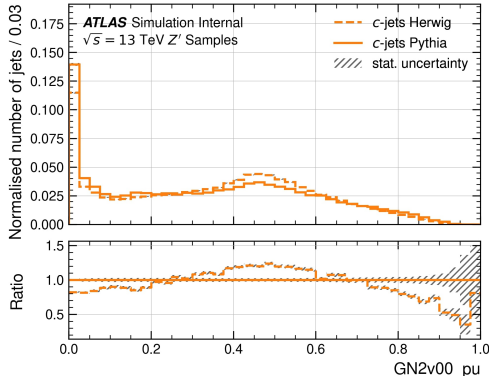
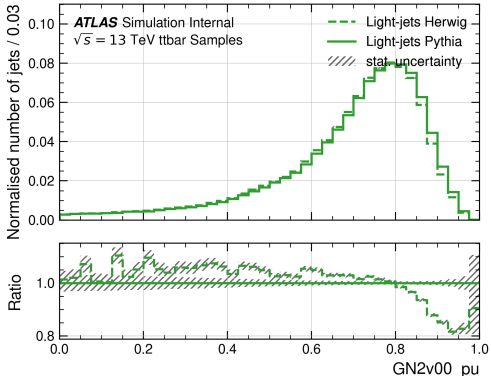
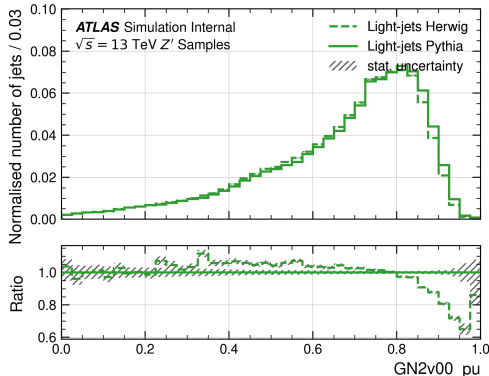
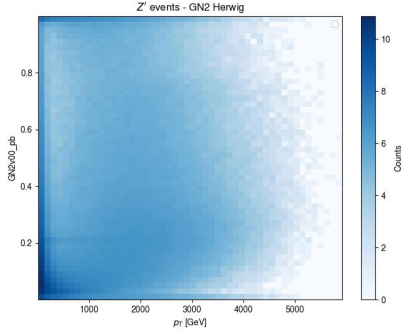
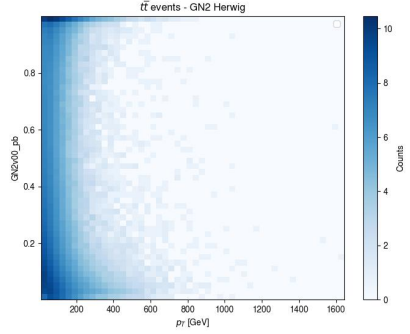
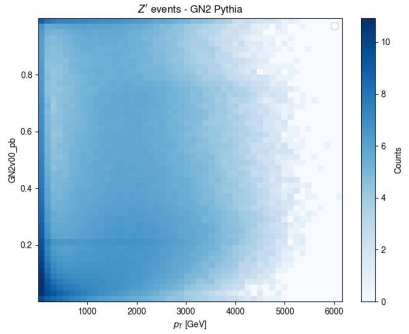
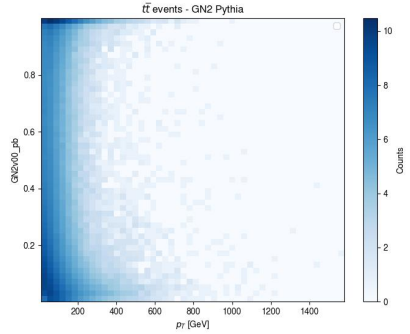
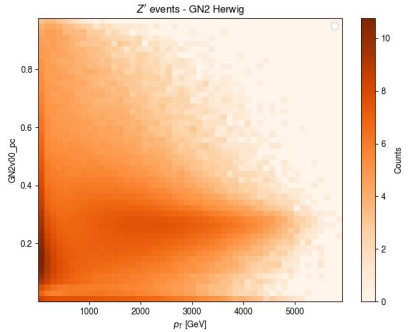
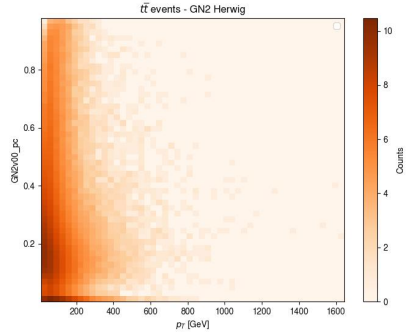
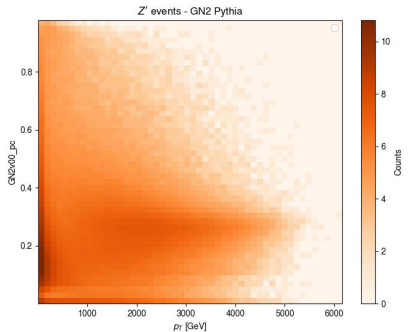
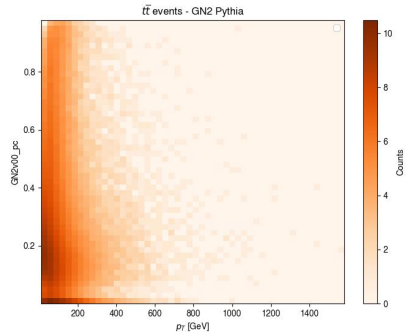
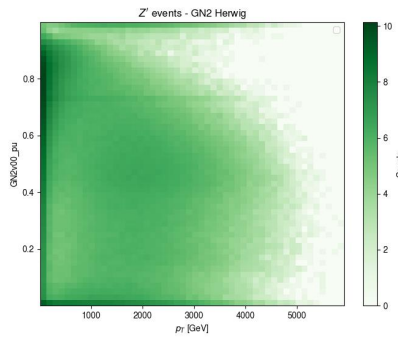
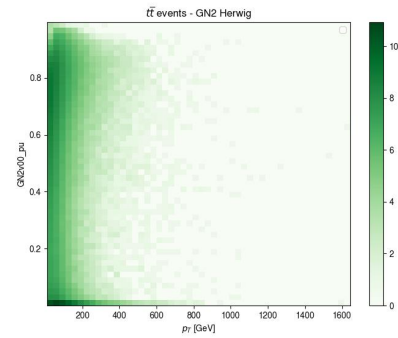
Description	$t\bar{t}$ Events	$Z'$ Events
<p>Herwig and Pythia b jets score u GN2v00_pu</p>		
<p>Herwig and Pythia c jets score u GN2v00_pu</p>		
<p>Herwig and Pythia u jets score u GN2v00_pu</p>		

Table 4. Scores Histograms for GN2v00\_pu

Description	$Z'$ Events	$t\bar{t}$ Events
<p>Histogram Herwig score b <math>p_T</math></p>		
<p>Histogram Pythia score b <math>p_T</math></p>		
<p>Histogram Herwig score c <math>p_T</math></p>		
<p>Histogram Pythia score c <math>p_T</math></p>		

Description	$Z'$ Events	$t\bar{t}$ Events
<p>Histogram Herwig score u <math>p_T</math></p>		
<p>Histogram Pythia score u <math>p_T</math></p>	